THE EUROPEAN
PHYSICAL JOURNAL C

Dark matter from freeze-in via the neutrino portal

Mathias Becker[a]

Fakultät für Physik, Technische Universität Dortmund, 44221 Dortmund, Germany

Abstract We investigate a minimal neutrino portal dark matter (DM) model where a right-handed neutrino both generates the observed neutrino masses and mediates between the SM and the dark sector, which consists of a fermion and a boson. In contrast to earlier work, we explore regions of the parameter space where DM is produced via freeze-in instead of freeze-out motivated by the small neutrino Yukawa couplings in case of $\mathcal{O}$ (TeV) heavy neutrinos. For a non-resonant production of DM, its energy density is independent of the DM mass. Assuming a democratic coupling structure we find $M_N \approx 10$ TeV. For the resonant production of DM, we find that it can be produced via freeze-in or freeze-out even with couplings of $\mathcal{O}(10^{-5})$. However, the measurement of the Lyman-α forest rules out the feeble coupled freeze-out case completely, while the resonant freeze-in production is only viable for $m_{DM} \gtrsim 3\,ke\mathring{V}$.

1 Introduction

Both dark matter (DM) and neutrino masses provide strong hints for beyond standard model physics (BSM). A way to accommodate neutrino masses is to introduce right-handed neutrinos as SM singlets, thereby allowing for mass generation via the type I seesaw mechanism.

Furthermore, the resulting heavy neutrino state N is massive and electrically neutral. If it is considered to be a DM candidate it must be stable. Thus, its mass must satisfy $M_N < 2m_e$. Therefore, the Yukawa coupling has to be very small, namely $y_\nu \lesssim 10^{-6}$. Consequently, the production rate is small, allowing for DM production via the freeze-in mechanism[1] [2,3].

In freeze-in scenarios, DM production never becomes efficient, i.e. the interaction rate Γ is always small compared to

the Hubble parameter H, $\Gamma \lesssim H$ (see Fig. 1). To account for the observed DM relic abundance via freeze-in of the decay $h \rightarrow N\nu$, the heavy neutrino mass should be of $\mathcal{O}(10\,\text{keV})$. However, the possibility of keV sterile neutrino DM via freeze-in within a minimal setup, the Dodelson-Widrow mechanism [4], is already excluded by the experiment, more precisely by the non-observation of the decay $N \rightarrow \nu\gamma$ [5,6] and Lyman-α measurements [7]. However, the idea of sterile neutrino dark matter via different production mechanisms continues to be widely discussed [8].

In case of $M_N > 2m_e$, the heavy neutrino N is obviously not stable and therefore not a DM candidate. But even in this case the right-handed neutrino can act as a mediator to DM since it is a SM singlet, a possibility which is referred to as *neutrino portal DM* (NPDM) [9–12].

Within these works, the small neutrino masses are generated by the type I seesaw mechanism and DM is produced via the freeze-out mechanism. In contrast, this work explores a minimal NPDM model where DM is produced via the freeze-in mechanism.

In Sect. 2, we introduce the particle content and the coupling structure of the model. In Sect. 3 the method for deriving the analytic results for the DM number density while assuming a thermal shape of the distribution function is introduced. Although those analytic results, which are discussed in Sect. 4, are not exact they allow for studying the parametrics for DM production. Following in Sect. 5 we numerically solve the Boltzmann equations at the level of momentum distribution functions taking the non-thermal form of the momentum distribution into account. Section 6 summarizes the relevant constraints on the model from direct detection, lepton flavour violation and structure formation. After that we conclude.

Within the appendices, the relevant reduced cross sections are given and the method for solving the boltzmann equations at the level of momentum distribution functions is discussed in more detail.

---

[1] A small DM production rate could also be generated by a large mediator mass as was pointed out in [1].

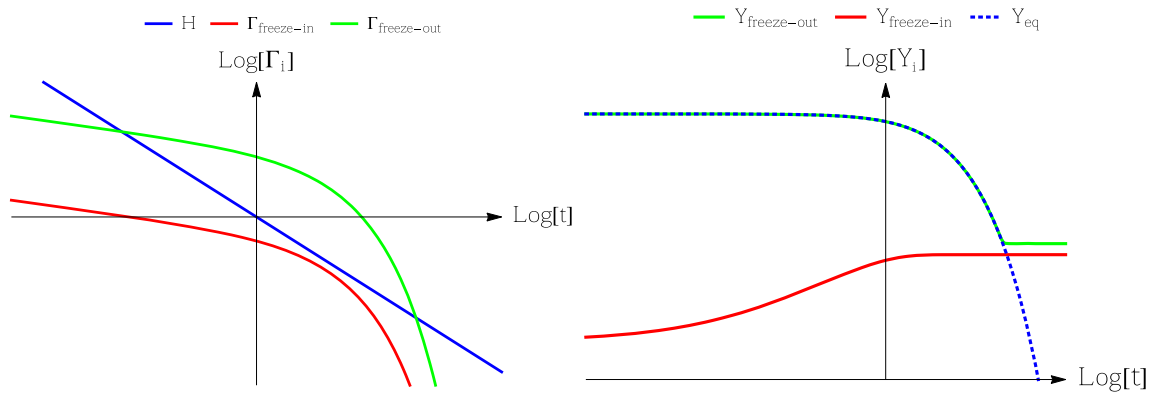[a] e-mail: mathias.becker@tu-dortmund.de

Fig. 1 Freeze-in and freeze-out scenarios in comparison: the left panel compares two interaction rates to the Hubble parameter H. Both of them are smaller than H for large temperatures since $\Gamma \sim T$ for $T \gg M$ and $H \sim T^2 M_{\text{Pl}}^{-1}$ and both interaction rates are exponentially suppressed for temperatures $T \sim M$, where M is the DM mass. The difference between the freeze-out case (green) and the freeze-in case (red) results from the much smaller coupling in the freeze-in case. The right panel shows the corresponding number densities compared to the equilibrium density in a co-moving volume

2 Setup

A model with similar particle content was investigated in [10], where DM production within freeze-out scenarios was explored. In addition to the SM particle content, the model includes three right-handed neutrinos ν_{R_i} to accommodate the observed neutrino masses. The dark sector consists of a fermion χ and a scalar ϕ. While they are uncharged under the SM gauge groups, they are charged under a dark symmetry, e.g. a dark U(1) or a $\mathcal{Z}_2$.[2] Assuming the SM particles to be uncharged under the dark symmetry renders the lighter particle of χ and ϕ to be a stable DM candidate since the dark symmetry forbids couplings between SM and dark sector particles. In this scenario, the resulting heavy neutrinos N_i mediate between the DM and the SM particles since the singlets ν_{R_i} can couple to $\bar{\chi}$ and ϕ via a Yukawa coupling as long as the expression $\bar{\chi}\phi$ is a singlet under all gauge groups. The parts of the Lagrangian relevant for the neutrino mass generation and the coupling to DM are given by

$$\mathcal{L} \supset - \underbrace{(Y_\nu)_{ij}\, \bar{\nu}_{L_i} h \nu_{R_j} - \frac{1}{2} (M_M)_{ij}\, \bar{\nu}_{R_i}^C \nu_{R_j}}_{\text{Neutrino mass generation}} - \underbrace{y_\chi \phi \bar{\chi} \nu_{R_i}}_{\text{DM coupling}} + h.c..$$

(2.1)

Here, we assumed a universal coupling of DM to the three right-handed neutrinos. Furthermore, we do not take into account any contribution to the DM relic abundance from a possible Higgs portal interaction arising from the term $(\phi\phi^*)(hh^*)$ in the scalar potential and additionally assume

that ϕ does not acquire a VEV. [3] Moreover, effects resulting from kinetic mixing of possible vector mediators of the dark symmetry with the SM gauge bosons are neglected. Thus, our analysis focuses on the neutrino portal to DM only.

After electroweak symmetry breaking the observed light neutrino masses are generated via the type I seesaw mechanism. To ensure that the observed neutrino masses and mixing angles are reproduced we utilize the following parametrization of the Yukawa coupling matrix Y_ν [15]:

$$\begin{aligned} Y_\nu &= \frac{\sqrt{M_N}}{v} R \sqrt{m_\nu} U_{\text{PMNS}}^\dagger \\ &= \underbrace{\frac{\sqrt{M_N \Delta m_\nu}}{v}}_{\equiv y_\nu} \underbrace{R \frac{1}{\sqrt{\Delta m_\nu}} \sqrt{m_\nu}}_{\equiv R'} U_{\text{PMNS}}^\dagger, \end{aligned}$$

(2.2)

where we assumed the Majorana mass matrix M_M to be diagonal with degenerated eigenvalues, i.e. $M_M = \text{diag}(M_N, M_N, M_N)$. U_{PMNS} is the PMNS matrix, v is the vacuum expectation value of the Higgs field, $\sqrt{m_\nu}$ is a diagonal matrix with the square root of the neutrino masses as eigenvalues, R is an orthogonal complex 3×3 matrix and Δm_ν is the square root of the large mass squared difference $\Delta m_\nu = \sqrt{\Delta m_\nu^2}$. The mass- and interaction eigenstates are transformed into each other in leading order in the small parameter $y_\nu v M_N^{-1}$ by the matrix U:

---

[2] For the calculation of the cross sections we use a real scalar. In this case DM stability is ensured by a $\mathcal{Z}_2$ symmetry.

[3] In fact, the validity of this assumption as well as the vacuum stability of this model will be investigated in a future work since due to a fermion loop consisting of a ν_R and a χ the ϕ mass term receives a negative contribution. In case the fermions in the loop are heavy compared to the boson those radiative corrections might lead to a negative m_ϕ^2 and thereby break the symmetry that stabilizes DM. Similar effects have been investigated for the scotogenic model [13,14] where those effects constrain the parameter space significantly.

$$\begin{pmatrix} \nu_L \\ \nu_R \end{pmatrix} = U \begin{pmatrix} \nu \\ N \end{pmatrix} \approx \begin{pmatrix} U_{\mathrm{PMNS}} & Y_\nu^T \nu M_N^{-1} \\ -Y_\nu U_{\mathrm{PMNS}} \nu M_N^{-1} & 1 \end{pmatrix} \begin{pmatrix} \nu \\ N \end{pmatrix} \tag{2.3}$$

The mixing between the left and right handed neutrinos causes an interaction between ν, N and the Higgs as well as a coupling of N to the $SU(2)_L$ gauge bosons. As presented in [16], the resulting interactions between the heavy and the light neutrinos are given by:

$$\mathcal{L}_W \supset -\frac{g_W}{2\sqrt{2}} l_i W_\mu^- \gamma^\mu (1-\gamma_5) B_{l_i N_j} N_j + h.c., \tag{2.4}$$

$$\begin{aligned} \mathcal{L}_Z \supset &-\frac{g_W}{4\cos(\Theta_W)} Z_\mu^0 \{ \bar{\nu}_i \gamma^\mu [i \mathrm{Im}(C_{\nu_i N_j}) \\ &- \gamma_5 \mathrm{Re}(C_{\nu_i N_j})] N_j \\ &\bar{N}_i \gamma^\mu [i \mathrm{Im}(C_{N_i N_j}) - \gamma_5 \mathrm{Re}(C_{N_i N_j})] N_j + h.c. \}, \end{aligned} \tag{2.5}$$

$$\begin{aligned} \mathcal{L}_H \supset &-\frac{g_W}{4 M_W} h \{ 2\bar{\nu}_i [(m_{\nu_i} + M_{N_j}) \mathrm{Re}(C_{\nu_i N_j}) \\ &+ i\gamma_5 (M_{N_j} - m_{\nu_j}) \mathrm{Im}(C_{\nu_i N_j})] N_j \\ &+ \bar{N}_i (M_{N_i} + M_{N_j}) \mathrm{Re}(C_{N_i N_j}) N_j \}. \end{aligned} \tag{2.6}$$

The matrices B and C are defined as in [16] and in case of real Yukawa couplings, as we will assume no CP violation from now on, they yield:

$$B_{l_i N_j} \approx \frac{\nu}{M_N} (Y_\nu^T)_{ij}, \quad C_{\nu_i N_j} \approx \frac{\nu}{M_N} (U_{\mathrm{PMNS}}^T Y_\nu^T)_{ij},$$

$$C_{N_i N_j} \approx \frac{\nu^2}{M_N^2} (Y_\nu Y_\nu^T)_{ij}. \tag{2.7}$$

Thus, the couplings relevant for heavy neutrino production are given by

$$\mathcal{L}_W \supset -\frac{M_W y_\nu}{\sqrt{2} M_N} (U_{\mathrm{PMNS}} R'^T)_{ij} \bar{l}_i W_\mu^- \gamma^\mu (1-\gamma_5) N_j + h.c., \tag{2.8}$$

$$\mathcal{L}_Z \supset \frac{M_W y_\nu}{2\cos(\Theta_W) M_N} (R'^T)_{ij} Z_\mu^0 \bar{\nu}_i \gamma^\mu \gamma_5 N_j, \tag{2.9}$$

$$\mathcal{L}_H \supset -y_\nu h (R'^T)_{ij} \bar{\nu}_i N_j - y_\nu^2 \frac{\nu}{M_N} h (R'^T R')_{ij} \bar{N}_i N_j, \tag{2.10}$$

whereas the coupling of the heavy neutrino to the dark sector is governed by:

$$\mathcal{L}_\chi \supset -y_\chi \phi \bar{\chi} N_i + h.c. \tag{2.11}$$

Note that the parameters y_ν and M_N are not independent and related by the seesaw mechanism requiring $y_\nu = \sqrt{\Delta m_\nu M_N} \nu^{-1}$. Therefore, the couplings in Eqs. (2.8)–(2.10) excluding the flavor dependent part can be rewritten as:

$$g_{h\nu N} = y_\nu = \frac{\sqrt{m_\nu M_N}}{\nu} \quad g_{WlN}, g_{Z\nu N} = y_\nu \frac{M_W}{M_N} = \sqrt{\frac{m_\nu}{M_N}} \frac{M_W}{\nu}$$

$$g_{hNN} = y_\nu^2 \frac{\nu}{M_N} = \frac{m_\nu}{\nu} \quad g_{ZNN} = g_{Z\nu N} \frac{y_\nu \nu}{M_N} = \frac{m_\nu}{M_N} \frac{M_W}{\nu} \tag{2.12}$$

Thus, for $M_N \geq M_W$, the coupling $g_{h\nu N}$ can be expected to be dominant and the $h\nu N$ vertex is the most relevant one for DM production. Whereas for $M_N \leq M_W$, the WlN and $Z\nu N$ vertices are expected to contribute the most to DM production as long as $M_N \gtrsim m_\nu$.

3 Boltzmann equations

Determining the relic abundance of the DM candidate requires solving the Boltzmann equations, which describe the time evolution of the particle number densities in the expanding universe. In principle, the boltzmann equations have to be solved at the level of momentum distribution functions, which then are integrated to obtain the number density. For a freeze-out production of DM however those distribution functions can be safely assumed to be proportional to a Boltzmann distribution, which allows for solving the Boltzmann equations at the level of number densities directly. Although this assumption can lead to less precise results in case of freeze-in production we will still use this formalism to obtain analytic expressions for the relic density in Sect. 4. Later on in Sect. 5, a numerical solution of the Boltzmann equation is given at the level of momentum distribution functions.

Here, we review the formalism for solving the Boltzmann equation for number densities, while the one for distribution functions is discussed in Appendix A.

Adopting the formalism used in [17], the Boltzmann equations can be written as

$$\begin{aligned} \dot{n}_N + 3H n_N = &-\sum_{a,i,j,\dots} \left(\frac{n_N n_a \cdots}{n_N^{\mathrm{eq}} n_a^{\mathrm{eq}} \cdots} \gamma_{\mathrm{eq}}(Na \cdots \to ij \cdots) \right. \\ &\left. -\frac{n_i n_j \cdots}{n_i^{\mathrm{eq}} n_j^{\mathrm{eq}} \cdots} \gamma_{\mathrm{eq}}(ij \cdots \to Na \cdots) \right). \end{aligned} \tag{3.1}$$

Here, n_i is the number density of particle species i. The $3H n_N$ term takes the expansion of the universe into account while the right hand side governs the impact of scattering processes which occur with a certain thermal rate γ_{eq}. The equilibrium number densities n_i^{eq} are given by the momentum integral over the distribution function f_i^{eq} of the respective particle species which is approximated with a Boltzmann distribution in our case:

$$n_i^{\mathrm{eq}} = \int \frac{d^3 p}{(2\pi)^3} f_i^{\mathrm{eq}} = \frac{g_i}{2\pi^2} m_i^2 T K_2 \left(\frac{m_i}{T} \right). \tag{3.2}$$

For a two to two scattering involving only CP conserving interactions the quantity γ_{eq} results in

$$\gamma_{eq}(Na \to ij) = \gamma_{eq}(ij \to Na)$$
$$= \frac{T}{64\pi^4} \int_{s_{min}}^{\infty} ds \sqrt{s}\hat{\sigma}(s) K_1\left(\frac{\sqrt{s}}{T}\right), \quad (3.3)$$

where $\hat{\sigma}(s) = 2s\,\sigma(s)\lambda\left[1, \frac{m_N^2}{s}, \frac{m_a^2}{s}\right]$ with $\lambda[a, b, c] = (a - b - c)^2 - 4bc$, $K_1(x)$ is a Bessel function and $s_{min} = \max[(m_a + M_N)^2, (m_i + m_j)^2]$.

Next, to simplify the form of the Boltzmann equations we write them in terms of the quantity $Y = \frac{n}{s_E}$, where $s_E = \frac{2\pi^2 g_{eff}^s}{45}T^3$ is the entropy density. This leads to

$$zHs_E\frac{dY_N}{dz} = -\sum_{a,i,j,\cdots} \gamma_{eq}(Na\cdots \leftrightarrow ij\ldots)$$
$$\times \left[\frac{n_N n_a \ldots}{n_N^{eq} n_a^{eq} \ldots} - \frac{n_i n_j \ldots}{n_i^{eq} n_j^{eq} \ldots}\right], \quad (3.4)$$

with $z = \frac{M_N}{T}$.

For the special case of freeze-in production via a two-to-two scattering process $b_1 b_2 \to ij$ the solution of this equation can be written in a compact form. Here, $b_{1/2}$ are particles in thermal equilibrium with the SM, whereas the number densities of i and j satisfy $n_{i/j} \ll n_{i/j}^{eq}$. Then, the Boltzmann equation for the particle species i is given by:

$$zHs_E\frac{dY_i}{dz} = \gamma_{eq}(b_1 b_2 \leftrightarrow ij). \quad (3.5)$$

Inserting γ_{eq} (3.3) and integrating the equation from very large temperatures, i.e. $z \to 0$, up to today, i.e. $z \to \infty$, yields:

$$Y_i = \frac{1}{64K m_i^4 \pi^4} \int_0^{\infty} dz\, z^3 \int_{s_{min}}^{\infty} ds\, \sqrt{s}\hat{\sigma}(s) K_1\left(\frac{\sqrt{s}}{m_i}z\right). \quad (3.6)$$

Here we use $K = Hs_E T^{-5}$ and $z = m_i T^{-1}$. After performing the z integration with the initial condition $Y_i(z = 0) = 0$ we are left with[4]

$$Y_i = \frac{3}{128K\pi^3} \int_{s_{min}}^{\infty} ds\, \frac{\hat{\sigma}(s)}{\sqrt{s^3}}. \quad (3.7)$$

---

[4] Equation (3.7) illustrates a behaviour typical for the freeze-in mechanism: assuming the reaction $b_1 b_2 \leftrightarrow ij$ involves a dominant mass scale M_{max} and noting that the mass dimension of the remaining integral is minus one yields $Y_i \sim M_{max}^{-1}$.
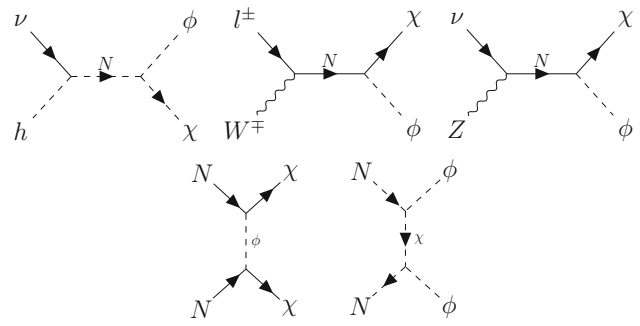

Fig. 2 Feynman diagrams for the DM production processes

4 Relic abundance: analytic estimates

The $2 \leftrightarrow 2$ scattering processes responsible for producing DM can be classified into two categories: *SM Particle Scattering* and *Heavy Neutrino Scattering*. The SM particle scattering processes involve two SM particles in the initial state, have χ and ϕ in the final state and are mediated by the heavy neutrino. Consequently, we have $\sigma \sim y_\nu^2 y_\chi^2$.

The heavy neutrino scattering processes have two heavy neutrinos in the initial state and produce a pair of χ or ϕ. Here, we have $\sigma \sim y_\chi^4$.

All contributing diagrams are displayed in Fig. 2. The following discussion assumes only one SM and right-handed neutrino generation. However, these results can easily be translated into a three generation setup due to the assumption of degenerated heavy neutrino masses, i.e. $M_{N_i} = M_N$ and the universal coupling of the dark sector to the right-handed neutrinos. For the heavy neutrino scattering, the one generation result has to be multiplied by a factor of nine. For the dominant SM particle scattering process $\nu_i h \to \chi\phi$ via a N_j the one generation contribution with a neutrino Yukawa coupling of $y_\nu = \sqrt{\Delta m_\nu M_N}v^{-1}$ has to be multiplied by $\sum_i |\sum_j (R'^T)_{ij}|^2 = f_1(\theta)$ where θ is a vector containing the in our case three real angles parametrizing the orthogonal matrix R. Choosing the standard parametrization for an orthogonal three by three matrix we find $10^{-16} \lesssim f_1(\theta) \leq 3$.

Since the $Z\nu_i N_j$ vertex has the same flavor structure as the $h\nu_i N_j$ vertex the one generation result for the $Z\nu$ initial state is multiplied by the same factor as the $h\nu$ initial state.

Only for the Wl initial the factor differs and results in $f_2(\theta) = \sum_i |\sum_j (U_{PMNS}R'^T)_{ij}|^2$. Here, we find $10^{-18} \lesssim f_2(\theta) \lesssim 7.65$. Scanning both f_1 and f_2 for randomly chosen values for the angles θ shows that on average $f_2 \approx 2.5 f_1$. Nevertheless, excluding the cases where f_1 is close to its lower bound, the contribution of the $h\nu_i$ initial state is still the dominant one due to the following reason: The production via the scattering of the gauge bosons is only viable for temperatures below the critical temperature where the $SU(2)_L \times U(1)_Y$ symmetry of the SM gets broken. Hence, the time of production is small compared to the Higgs neu-

trino scattering. Therefore, we consider only the production via $h\nu_i \to \chi\phi$ for the analytic estimates, while all production channels are taken into account in the numerical solution.

4.1 SM particle scattering

For the rest of the discussion, we assume that the dark sector particles have roughly the same mass and replace $m_\phi = m_\chi$. The reduced cross section for the dominant production channel is given by:

$$\sigma_{\nu h \leftrightarrow \chi\phi}(s) = y_\chi^2 y_\nu^2 \frac{\left(1 - \frac{m_h^2}{s}\right) s^2 \sqrt{\left(1 - 4\frac{m_\chi^2}{s}\right)}}{16\pi[(s - M_N^2)^2 + \Gamma_N^2 M_N^2]}. \tag{4.1}$$

Here, Γ_N is the total decay width of the propagating neutrino. There are two cases to be distinguished:

- The resonant case with $M_N \geq 2m_\chi$ where $M_N^2 \geq s_{\min}$.
- The non-resonant case with $M_N < 2m_\chi$ where $M_N^2 < s_{\min}$.

First, we discuss the non-resonant case. If we neglect the contribution of the Higgs mass, i.e. $m_h \ll m_\chi$, we can use Eq. (3.7) to determine the relic density directly:

$$Y_{\mathrm{DM}} = Y_\chi + Y_\phi$$
$$= \frac{3^4}{2^{11}\pi^5} \frac{y_\nu^2 y_\chi^2}{\sqrt{g_{\mathrm{eff}}} g_{\mathrm{eff}}^s} \frac{M_{\mathrm{pl}}}{\sqrt[4]{[4m_\chi^2 - M_N^2]^2 + \Gamma_N^2 M_N^2}} \tag{4.2}$$

$$\overset{M_N \ll m_\chi}{=} \frac{3^4}{2^{12}\pi^5} \frac{y_\nu^2 y_\chi^2}{\sqrt{g_{\mathrm{eff}}} g_{\mathrm{eff}}^s} \frac{M_{\mathrm{pl}}}{m_\chi}, \tag{4.3}$$

where $g_{\mathrm{eff}}^{(s)}$ are the number of effective relativistic (entropy) degrees of freedom which are both assumed to be constant during this calculation with $g_{\mathrm{eff}}^{(s)} = 106.75$.[5] Note that for obtaining this result the reduced cross section was multiplied by an additional factor of four arising from the four degrees of freedom of the Higgs doublet before the electroweak phase transition.

Remarkably in case of a heavy DM mass m_χ compared to the mediator mass M_N, the result is inversely proportional to the DM mass, i.e. the energy density is independent of m_χ. This allows for predicting the value of the product of the Yukawa couplings $y_\nu y_\chi$ by setting $Y_{DM}(z \to \infty) = Y_{DM,\exp}$, with

$$Y_{DM,\exp} = \frac{\Omega_{DM}}{\Omega_B} \frac{m_B}{m_{DM}} Y_B \approx 10^{-10} m_B m_\chi^{-1}. \tag{4.4}$$

The experimental values for Ω_{DM}, the density parameter for baryons Ω_B, and the baryon number density in a co-moving volume Y_B, are taken from [18] and m_B, the average baryon mass, is approximated with the proton mass.

Evaluating $Y_{DM} = Y_{DM,\exp}$ results in:

$$(y_\nu y_\chi)^2 \approx 10^{-3} \frac{m_B}{M_{\mathrm{Pl}}} \approx 10^{-21}. \tag{4.5}$$

The implications of this result are discussed in Sect. 4.3

Next, we discuss the resonant case, i.e. $M_N \geq 2m_\chi$. As it was pointed out in [19], in this case it is useful to approximate the Breit-Wigner peak in Eq. (4.1) with:

$$\int_c^\infty dx \frac{f(x)}{(x-a)^2 + b^2} \approx \frac{f(a)}{b}, \tag{4.6}$$

which is valid as long as $b \ll a$, i.e. $\Gamma_N \ll M_N$. Then, the integration of Eq. (3.7) results in:

$$Y_{DM}(z \to \infty) = \frac{27}{4\pi^5 g_{\mathrm{eff}}^s \sqrt{g_{\mathrm{eff}}}} \frac{(y_\nu y_\chi)^2}{y_\nu^2 + y_\chi^2} \frac{M_{\mathrm{pl}}}{M_N}, \tag{4.7}$$

where we already used $M_N \gg m_\chi$ to simplify the result. Again, we postpone the discussion of the result to Sect. 4.3.

4.2 Heavy neutrino scattering

The cross sections for the heavy neutrino scattering for the case of $M_N \ll m_\chi$ result in

$$\sigma_{NN \to \chi\chi} = y_\chi^4 \frac{\sqrt{1 - \frac{4m_\chi^2}{s}}}{8\pi s}, \tag{4.8}$$

$$\sigma_{NN \to \phi\phi} = \frac{y_\chi^4}{2\pi} \left[\left(1 + 4\frac{m_\chi^2}{s}\right) \log \right.$$
$$\left. \times \left(\frac{s - 2m_\chi^2 - \sqrt{s^2 - sm_\chi^2}}{2m_\chi^2}\right) + 2\sqrt{1 - 4\frac{m_\chi^2}{s}} \right]. \tag{4.9}$$

By again employing Eq. (3.7) we find:

$$Y_{\mathrm{DM}} = Y_\chi + Y_\phi = \frac{35 \cdot 3^3 y_\chi^4}{2^{13}\pi^5 \sqrt{g_{\mathrm{eff}}} g_{\mathrm{eff}}^s} \frac{M_{\mathrm{Pl}}}{m_\chi}. \tag{4.10}$$

As for the SM particle scattering in the limit of $M_N \ll m_\chi$, the DM density is inversely proportional to its mass.

For the case where the SM scattering processes are in the resonant regime, i.e. $M_N > 2m_\chi$, in the limit $M_N \gg m_\chi$ we cannot find an analytic estimate for the DM relic density beside

$$Y_{\mathrm{DM}} \sim \frac{y_\chi^4 M_{\mathrm{Pl}}}{\sqrt{g_{\mathrm{eff}}} g_{\mathrm{eff}}^s M_N}. \tag{4.11}$$

---

[5] This is a good approximation as long as the production is mainly efficient for temperatures above 100 GeV.

Although the factor of proportionality is unknown we expect this to be much smaller compared to the contribution of the SM particle scattering. This is due to the resonance contributing to the production via SM particle scattering. Hence, we neglect this contribution for the discussion of the analytic results.

4.3 Discussion of the analytic results

In the limit of $M_N \ll m_\chi \approx m_\phi$ we found analytic solutions for the DM relic density for both types of processes. Combining both results yields:

$$Y_{DM}(z \to \infty) = \frac{3^3}{2^{13}\pi^5 g_{\text{eff}}^s \sqrt{g_{\text{eff}}}} \frac{M_{\text{Pl}}}{m_\chi}(6y_\nu^2 y_\chi^2 + 35y_\chi^4).$$
(4.12)

By comparing this expression with the observed DM density (4.4) one obtains

$$(6y_\nu^2 y_\chi^2 + 35y_\chi^4) \approx 10^{-21}.$$
(4.13)

Since the coupling y_ν is only a function of M_N the coupling y_χ is fixed by the heavy neutrino mass M_N. Moreover, we find $y_\chi \lesssim 10^{-5}$ in order not to overproduce DM.

In principle, the couplings y_χ and y_ν are otherwise unrelated. However, both describe a coupling to the right-handed neutrino and – if the heavy neutrino is lighter than $\mathcal{O}(10^{15}\,\text{GeV})$ – both couplings are required to be relatively small. This motivates the idea that they might be suppressed by the same mechanism, resulting in $y_\nu \approx y_\chi$.[6] Considering a model which generates $y_\chi \approx y_\nu$ allows for constraining the mass of the heavy neutrino since then Eq. (4.13) reads

$$41y_\nu^4 = 41\left(\frac{m_\nu M_N}{v^2}\right)^2 \approx 10^{-21}.$$
(4.14)

Thus, to fit the observed DM density (4.4), $M_N \approx 10\,\text{TeV}$ is required. Since we are investigating the non-resonant regime we have $M_N < 2m_{\text{DM}}$. Therefore, we find a lower bound on the DM mass of $m_{\text{DM}} \gtrsim 5\,\text{TeV}$ if we naively assume the behaviour for large DM masses to be also correct for parameters close to the transition of the non-resonant to resonant regime.

We achieved this result by assuming $n_N = n_N^{\text{eq}}$, $m_\chi \gg M_N$ and by only taking into account the dominant processes of the SM particle scattering. From Eq. (4.12), we see that the contribution of the heavy neutrino scattering processes

accounts for roughly eighty percent of the produced DM in case of $y_\chi = y_\nu$. Thus, the result will be altered significantly if the heavy neutrinos are out of equilibrium during the time where the production via heavy neutrino scattering is efficient. Also, we expect a significant change in areas of the parameter space where $m_\chi \approx M_N$, whereas taking into account the sub-dominant processes does not have a significant impact since they are suppressed by $\frac{M_W^2}{M_N^2}$ and only accessible after electroweak symmetry breaking. For these reasons, we solve the Boltzmann equations numerically for various coupling structures in Sect. 5.

Additionally, we found an analytic solution for the DM relic density in the limit $M_N \gg m_\chi$ where the SM particle scattering processes are in the resonant regime:

$$Y_{DM}(z \to \infty) = \frac{27}{4\pi^5 g_{\text{eff}}^s \sqrt{g_{\text{eff}}}} \frac{(y_\nu y_\chi)^2}{y_\nu^2 + y_\chi^2} \frac{M_{\text{pl}}}{M_N}.$$
(4.15)

In case of $y_\chi \ll y_\nu$ we find the observed DM energy density if $y_\chi \approx 10^{-12}\sqrt{\frac{M_N}{m_\chi}}$.

However, if $y_\chi \ll y_\nu$ does not hold the approximation of $n_\chi \ll n_\chi^{\text{eq}}$ we used to derive (4.12) does not apply anymore. To illustrate that we look at the case $y_\chi = y_\nu$, where (4.12) results in:

$$Y_{DM}(z \to \infty) \approx \frac{3^3}{2^2\pi^5 g_{\text{eff}}^s \sqrt{g_{\text{eff}}}} \frac{m_\nu M_{\text{Pl}}}{v^2} \approx 10^{-1}.$$
(4.16)

Using Eq. (3.2) we find that $Y_{DM}^{\text{eq}} \lesssim 10^{-2}$. Therefore, $n_\chi \ll n_\chi^{\text{eq}}$ cannot be satisfied. Hence, the freeze-in scenario does not apply here. Nevertheless, it is still possible to account for the correct amount of DM. In this case, we recover a freeze-out like scenario since due to the resonance the interaction rate becomes as large as the Hubble parameter although the system is feebly coupled. Thus, DM comes into equilibrium with the SM and freezes out as soon as the interaction rate becomes smaller than the Hubble parameter. This occurs approximately at $T = M_N$.[7] Consequently, the number density can be estimated by the equilibrium density at freeze-out:

$$Y_{DM}(z \to \infty) = Y_\chi^{\text{eq}}(T \approx M_N) \overset{M_N \gg m_\chi}{=} \frac{45g_\chi}{2\pi^4 g_{\text{eff}}^s} \approx 10^{-3}.$$
(4.17)

Equating this result with Eq. (4.4) yields a DM mass of $m_\chi = \mathcal{O}(100\,\text{eV})$. In contrast to the non-resonant case, this DM mass violates the Tremaine–Gunn bound which

---

[6] For example, such a mechanism could be an extra dimensional model where the right-handed neutrino in contrast to all other particles propagates in an extra dimension since it is uncharged under all considered gauge groups. Thereby, its coupling gets suppressed by the reduced wave function overlap [20,21].

[7] This is due to the fact that the main contribution to the interaction rate comes from the resonance at $s = M_N^2$, i.e. as soon as the temperature drops below M_N the resonance cannot be reached efficiently anymore and therefore the interaction rate decreases significantly.
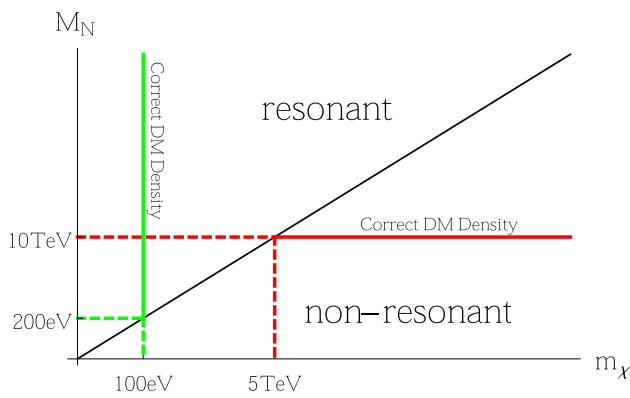
Fig. 3 Parameter space for $y_\chi = y_\nu$: the black line divides the plane spanned by the DM mass m_χ and the mediator mass M_N into two halves. The upper (lower) half corresponds to the resonant (non-resonant) DM production regime. The red and green line show where the correct amount of DM is produced for the non-resonant and the resonant regime, respectively. In the non-resonant regime, producing the correct density only depends on the mediator mass, whereas it only depends on the DM mass in the resonant region

Fig. 4 The numerically obtained DM density Y_{th} is compared to the observed DM density Y_{exp} for different values of the DM mass m_χ and the mediator mass M_N: the different colored solid lines represent the points where the observed DM density is reproduced for a certain coupling structure. A parameter point above a specific line overproduces DM for the corresponding coupling structure while points below do not generate enough DM. Lines of the same color have the same coupling structure. A solid line represents a scenario with of $f_1(\theta) = 1$, while a dotted represents a scenario with $f_1(\theta) = 0.1$. The black line separates the plane into the non-resonant (lower right) and resonant (upper left) regime. The latter one was not scanned. We assumed normal ordering and one massless neutrino

restricts fermionic DM to have a mass of at least roughly a keV [22]. Therefore, DM must be bosonic in this case. However, this case also is in tension with observations of the Lyman-α forest which allows to probe structures of the size $10^{0-2}h^{-1}$ Mpc [23]. This issue is treated in more detail within Sect. 6.

We summarized our results for the case $y_\chi = y_\nu$ in a schematic plot (see Fig. 3).

5 Numerical analysis

We solved the Boltzmann equations numerically in the non-resonant case for different coupling structures $y_\chi = (0.1, 1, 10)y_\nu$ and DM masses of $m_\chi \in [10^2, 10^{10}]$ GeV assuming different flavor structures, i.e. $f_1(\theta) = (10^{-1}, 1)$ and $f_2(\theta) = 2.46$ and a normal mass hierarchy in the neutrino sector, i.e. $m_{\nu_1} < m_{\nu_2} < m_{\nu_3}$. Additionally, we set $m_{\nu_1} = 0$ in the results presented in Fig. 4.

Since we investigate a feebly coupled sector, the back reactions in the DM production processes can be neglected. Only for the processes $N \leftrightarrow \nu h$ responsible for producing the mediator N the back reactions are relevant, since for most of the parameter space N equilbrates with the SM.

Therefore, we solve the Boltzmann equation in two steps:

1. The N production via $N \leftrightarrow \nu h$ is solved at the level of the momentum distribution function, thereby taking into account the non-thermal shape of the distribution. The details of solving the Boltzmann equations at the level of momentum distribution functions are given in Appendix A and th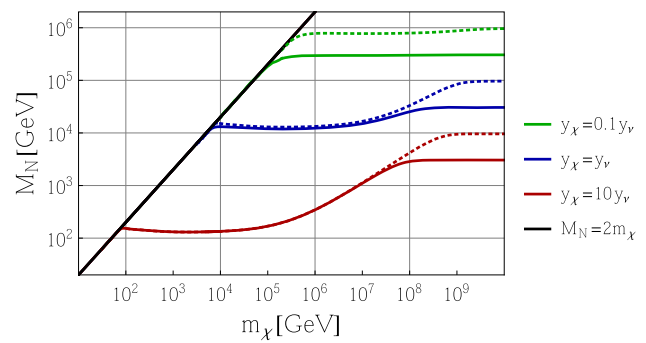e collision term for the process in question is given in Eq. (A.23). Eventually, this procedure results in the quantity $\frac{n_N}{n_N^{eq}}(T)$.[8] We take $\frac{n_N}{n_N^{eq}}(T \to \infty) = 0$ as initial condition.

2. This quantity is used to solve the Boltzmann equations for DM production via heavy neutrino and SM particle scattering employing the formalism described in Sect. 3. We take vanishing number densities for the DM particles as initial conditions. The SM particles are assumed to follow their equilibrium densities throughout the production process. The final result is then given by $Y_{DM} = Y_\chi + Y_\phi$ for $T \to 0$. Note that the independent solution of the Boltzmann equations for the dark sector particles and the heavy neutrino is only possible due to the tiny interaction rate, which allows to neglect the back reactions from DM production via heavy neutrino scattering.

The results are summarized within Fig. 4. From our earlier considerations in Sect. 4.3 we expect the setup to work for a constant mediator mass M_N as long as $m_\chi \gg M_N$. This constant value can be obtained by solving Eq. (4.13) for a given coupling structure. Consider e.g. the case $y_\nu = y_\chi$, where Eq. (4.13) results in $M_N \approx 10$ TeV. This case is illustrated by the solid blue line in Fig. 4. For 10 TeV $\leq m_\chi \leq 10^4$ TeV the prediction is met by the numerical solution. For larger DM masses, however, a larger mediator mass is required to accommodate the observed relic density. This is due to the following reason: The freeze-in mechanism produces DM efficiently down to temperatures around the heaviest mass

---

[8] Note that the quantity n_N is defined as the sum over all three heavy neutrinos, i.e. $n_N = \sum_j n_{N_j}$.
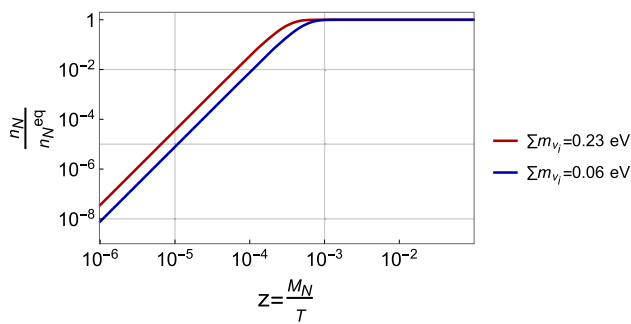
Fig. 5 The ratio of the heavy neutrino density to its equilibrium density against the dimensionless quantity $z = M_N T^{-1}$ in case of $\sum_i m_{\nu_i} = 0.06\,\text{eV}$ ($\sum_i m_{\nu_i} = 0.23\,\text{eV}$) [24], corresponding to the lower (upper) bound on the sum of the three active neutrino masses. Since the production rate of N is proportional to the sum of the active neutrino masses this choice shows the earliest and latest point of equilibration. The heavy neutrinos reach equilibrium for $T \approx 10^3 M_N$ in both cases. In Fig. 4, the lower bound on the sum of the neutrino masses was used, but the results are negligibly different when considering the upper bound

involved in the production process. For the non-resonant regime this mass is given by the DM mass itself. Therefore, DM production is efficient for $T \gtrsim m_\chi$. The mediator mass and, thereby the neutrino Yukawa y_ν, start to increase as soon as $\frac{n_N}{n_N^{\text{eq}}}(T) \ll 1$ for $T \gtrsim m_\chi$, since this suppresses DM production via heavy neutrino scattering. In case of $y_\nu = y_\chi$ heavy neutrino scattering accounts for $\frac{35}{41}$ of the DM production if the heavy neutrinos are following their equilibrium density during the time of production. If this contribution is missing, it has to be compensated by a larger neutrino Yukawa which results in a larger mediator mass.

The heavy neutrinos reach thermal equilibrium with the SM via the inverse decay $\nu_i h \rightarrow N_j$ for $T \sim c M_N$. The factor c is independent of the neutrino Yukawa y_ν and the parameters θ which encode the flavor structure of the neutrino Yukawas. However, it depends on the sum of the three active neutrino masses since the decay rate is proportional to this sum. The evolution of the heavy neutrino number density is shown in Fig. 5. Here, the heavy neutrinos reach equilibrium for $T \approx 10^{-3} M_N$. Therefore, the lines in Fig. 4 start to deviate significantly from a constant value of M_N for $m_\chi > 10^3 M_N$, since in this case it is $\frac{n_N}{n_N^{\text{eq}}}(T) < 1$ for the complete production time. A constant value of M_N is reached again if the contribution of the heavy neutrino scattering becomes negligible.

For $f_1 = 0.1$ the contribution of SM particle scattering is suppressed by a factor of 10 since the contribution of the SM particle scattering is proportional to f_1. Thus, a larger coupling compared to $f_1 = 1$ is required. This effect can be seen in Fig. 4 where all dotted lines lie above the solid line of the same color.

The different couplings structures result in larger (smaller) mediator masses for a small (large) dark Yukawa coupling compared to the neutrino Yukawa. Additionally, the effect of a small f_1 differs for a small (large) dark Yukawa. While the increase with a larger DM mass becomes less significant for a small dark Yukawa, the absolute difference between the small and large f_1 cases becomes stronger. This is due to the different contributions from heavy neutrino and SM particle scattering for the different coupling structures.

For smaller DM masses close to the transition to the resonant regime, the correct DM relic density is obtained for values of M_N very close to $M_N = 2m_\chi$. Although not visible within Fig. 4, all lines follow the black line down to small DM masses until the enhancement close to the resonance is not strong enough anymore to generate a sufficient amount of DM. However, the numerical solution is not trustworthy in this area due to numerical instabilities and therefore not presented here. We estimate the lower bound on m_χ by evaluating Eq. (4.2) in the limit $M_N \rightarrow 2m_\chi$. In the case of $y_\chi = \alpha y_\nu$ we obtain $m_\chi \gtrsim \alpha^{-\frac{4}{3}}\,\text{MeV}$.

6 Constraints

In this section we discuss different constraints on the model. At first we discuss constraints from structure formation which pose strong limits in the resonant regime. Afterwards we investigate the impact of direct detection bounds on our parameter space and briefly discuss charged lepton flavor violation and indirect detection.

6.1 Structure formation

Since DM particles only interact weakly with the SM they can escape from gravitational wells formed in the early universe, thereby delaying structure formation below their free-streaming scale. Given the redshift at the production time z_{prod} the free-streaming scale is given by

$$\lambda_{fs} = \int_0^{z_{\text{prod}}} dz \frac{v(z)}{H(z)}, \tag{6.1}$$

where $v(z)$ is the DM velocity at a given redshift z.

The observation of absorption lines in the spectra of distant quasars mostly induced by hydrogen clouds, the so called Lyman-α forest, allows for probing structures on the scale of roughly $10^{0-2} h^{-1}\text{Mpc}$ [23].

Following the lines of [25], we estimate the free-streaming scale for the case of DM in equilibrium with the SM up to a certain freeze-out temperature and for the case of resonantly produced DM still in the freeze-in regime. Within this model,

the first case applies to the resonant production with a coupling structure of $y_\nu \lesssim y_\chi$ whereas the latter is present in the resonant production regime for $y_\chi \ll y_\nu$. The non-resonant production regime is not investigated here due to the much larger DM masses that are required to generate the observed relic density. Therefore, we do not expect this case to be in tension with the Lyman-α forest.

As it was pointed out in [26], the free-streaming scale should only be understood as an order-of-magnitude estimator in the case of non-thermal DM momentum distribution and may differ up to $\mathcal{O}(1)$ factors from results obtained with dedicated tools like the CLASS-code which computes the linear matter power spectrum.

For the purposes of this work, the estimation of the free-streaming length suffices, firstly because the non-thermal momentum distribution produced by the resonant freeze-in process (Eq. (A.21)) is close to a thermal shape and secondly because the resonantly produced DM for the freeze-out case will be excluded by this method by roughly two orders-of-magnitude.

We approximate the velocity in Eq. (6.1) by the average velocity at the production time z_{prod} which is only redshifted afterwards, i.e.

$$v(z) = \frac{p(z)}{\sqrt{p(z)^2 + m_\chi^2}}, \tag{6.2}$$

with

$$p(z) = p_{\mathrm{prod}} \frac{1+z}{1+z_{\mathrm{prod}}}, \tag{6.3}$$

and

$$p_{\mathrm{prod}} = \frac{\int dp\, p^3 f(p, T_{\mathrm{prod}})}{\int dp\, p^2 f(p, T_{\mathrm{prod}})}. \tag{6.4}$$

Moreover, the Hubble parameter is given by

$$H(z) = H_0 \sqrt{\Omega_m (1+z)^3 + \Omega_r (1+z)^4 + \Omega_\Lambda}. \tag{6.5}$$

For the numerical evaluation, we use the cosmological parameters of [27]. Lastly, we use the relation between the temperature and the redshift $T = T_0 (1+z) \left(\frac{g_s^{\mathrm{eff}}(T_0)}{g_s^{\mathrm{eff}}(T)} \right)^{\frac{1}{3}}$ to give T_{prod} in terms of the redshift. The temperature T_0 refers to the temperature today. Inserting these expressions into (6.1) allows for calculating λ_{fs} in terms of the production time z_{prod} and the average momentum at this time p_{prod}. Then, the result is compared to the upper bound on the free-streaming scale of $\lambda_{fs} \lesssim 0.1$ Mpc which was derived in [25] assuming that the particle species in question accounts for all of the observed DM relic density.

In case of resonant production with $y_\nu \lesssim y_\chi$ we can assume DM to have a Boltzmann like momentum distribution, i.e. $f(p, T) = \exp(-E_p T^{-1})$. We take the time of production to be the freeze-out temperature since the interactions of DM with the SM cease to be efficient from this point on. For this distribution the average momentum results in

$$p_{\mathrm{prod}} = \frac{m_\chi^2 + 3 m_\chi T_{\mathrm{prod}} + 3 T_{\mathrm{prod}}^2}{m_\chi + T_{\mathrm{prod}}}. \tag{6.6}$$

By comparing the interaction rate Γ of the process $\nu h \to \chi \phi$ in the resonant regime to the Hubble parameter we find that $T_{\mathrm{prod}} \approx M_N$. For mediator masses $M_N \gtrsim$ MeV the free-streaming scale becomes insensitive to the mediator mass itself beside the change induced by the different $g_S^{\mathrm{eff}}(T_{\mathrm{prod}})$. In this case, we find a lower bound on the DM mass of $m_\chi \gtrsim 10$ keV. However, we found in Sect. 4.3 that a DM mass of 0.1 keV is required in order not to overproduce DM within this scenario. This lies two orders of magnitude below the estimated lower bound. Therefore, the resonant production regime with $y_\nu \lesssim y_\chi$ is excluded by the Lyman-α measurement.

If, on the other hand, $y_\chi \ll y_\nu$, DM does not equilbrate with the SM even in the resonant production regime. Therefore the spectrum is non-thermal and given by Eq. (A.21). We take $z_{\mathrm{prod}}(T_{\mathrm{prod}})$ as the temperature where the derivative of the total particle number with respect to the time is maximized. Therewith, we find $T_{\mathrm{prod}} = 3.36 M_N$ which results in $p_{\mathrm{prod}} = 0.4 T_{\mathrm{prod}}$. Here, we also find that for $M_N \gg m_\chi$ the free-streaming scale is insensitive to the mediator mass and the lower bound on the mass results in $m_\chi \gtrsim 3$ keV.

To summarize, the Lyman-α measurement strongly constraints the resonant production regime of this model. While the case where the resonant enhancement of the production cross section is strong enough to equilibrate DM with the SM is completely ruled out, the freeze-in regime is only allowed for couplings $y_\chi \lesssim 10^{-12} \sqrt{\frac{M_N}{\mathrm{keV}}}$ with $m_\chi \gtrsim 3$ keV.

6.2 Direct detection

Direct detection experiments search for interactions of DM with nuclei. In this model, a coupling of DM to the Z boson is generated at one loop. The corresponding Feynman diagram is shown in Fig. 6. The coupling to the Z is then given by $\mathcal{L} \supset g_{Z\chi\chi} \bar{\chi} \gamma^\mu P_L \chi Z_\mu$ with [28]

$$g_{Z\chi\chi} = -\frac{y_\chi^2}{16\pi^2} \frac{g_w}{4 \cos\theta_w} \frac{\Delta m_\nu}{M_N} 2.3 \cdot g\left(\frac{M_N^2}{m_\phi^2} \right), \tag{6.7}$$
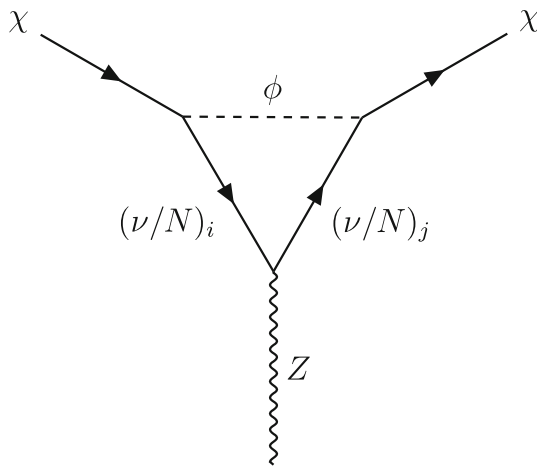
Fig. 6 1-Loop diagram generating the effective coupling of DM to the Z. The indices i, j run from 1 to 3

Fig. 7 The expected direct detection signals for the coupling structures investigated within Sect. 5 are compared to the current bounds from XENON1T [33] (dashed black curve). The dip in the red curve is due to a cancellation appearing in the loop function

and

$$g(x) = \frac{x[(x+2)\log(x) + 3(1-x)]}{2(1-x)^2},$$ (6.8)

where we have used the best fit values of [29] for the parameters of the PMNS matrix in case of normal ordering, which yields $\sum_{k,m=1}^{3}(Y_\nu^T Y_\nu)_{km} \approx 2.3 \cdot y_\nu^2$.

Therewith, DM interacts with quarks via Z exchange. Since this process happens at energies far below the Z mass, the heavy mediator is integrated out leading to

$$\mathcal{L} \supset \frac{1}{M_Z^2}[g_{Z\chi\chi}\bar{\chi}\gamma^\mu(1-\gamma^5)\chi][\bar{q}\gamma_\mu(g_{qv}+g_{qa}\gamma^5)q],$$ (6.9)

where g_{qv} and g_{qa} are the couplings of the SM quarks to the Z. At low energies only the vector-vector and axial-axial interactions are not suppressed by powers of the relative velocity or momentum transfer, thereby leading to a spin-independent and a spin-dependent DM-nuclei cross section, respectively [30,31]. For the spin-independent cross section we obtain [31]

$$\sigma_{SI} = \frac{\mu_{\chi N}^2 g_{Z\chi\chi}^2}{\pi M_Z^4}[Z(2g_{uv}+g_{dv}) + (A-Z)(g_{uv}+2g_{dv})],$$ (6.10)

with $\mu_{\chi N} = \frac{m_\chi M_{Xe}}{m_\chi + M_{Xe}}$, $g_{uv} = g_w\left(\frac{1}{4\cos\theta_w} - \frac{2\sin^2\theta_w}{3\cos\theta_w}\right)$ and $g_{dv} = g_w\left(-\frac{1}{4\cos\theta_w} + \frac{\sin^2\theta_w}{3\cos\theta_w}\right)$.

This cross section is constrained by the XENON experiment, as shown in Fig. 7. Therefore, the freeze-in setup cannot be constrained by this measurement. There are scenarios considered in the literature which allow for having a large direct detection signature even in a freeze-in scenario [32].
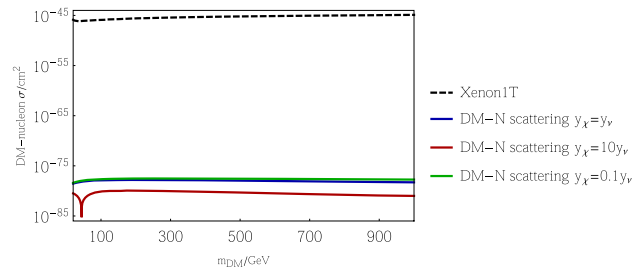
In [32], the cross section is enhanced due to a very light mediator. Since in our model the interaction is mediated by a Z boson this does not apply here.

6.3 Indirect detection and HEP phenomenology

Prospects for indirect detection of DM such as the observations of γ-rays from the galactic center or the precise measurement of the CMB all rely on the efficient annihilation of DM into SM particles. In the case of neutrino portal DM this usually happens subsequently by DM first annihilating into heavy neutrinos which then decay or annihilate into SM particles. Several prospects for indirect detection were investigated in [34] for the case of freeze-out production of DM where before DM freezes out its annihilation is efficient. This, however, is not the case for the freeze-in scenario investigated in this work. Here, the process is efficient only in the direction of DM production. This leads to a suppression of the annihilation cross section $\langle\sigma v\rangle$ which enters all observables of indirect detection considered in [34] since the couplings y_ν and y_χ are required to be feeble. Moreover, the annihilation rate is suppressed by a factor $\frac{n_{DM}^{eq}}{n_{DM}}$ compared to the freeze-out case. For this reason we do not study indirect detection observables within this work.

The minimal version of the type I seesaw mechanism employed here induces couplings of the SM gauge bosons and the Higgs to the heavy neutrino states. This can modify electroweak precision observables and induce charged lepton flavor violation (LFV) as well as additional Higgs decay channels in case of a light heavy neutrino [35,36]. The strongest constraints come from the decay $\mu \to e\gamma$ with $\mathcal{B}(\mu \to e\gamma) \leq 4.2 \cdot 10^{-13}$ [24]. Within this setup the decay is mediated at one loop level by a W boson and a neutrino. The branching ratio of this process is then given by [37]:

$$\frac{\Gamma(\mu \to e\gamma)}{\Gamma(\mu \to \nu_\mu e\bar{\nu}_e)} = \frac{3\alpha}{32\pi}\frac{\left|\sum_{k=1}^{6} U_{\mu k}U_{ek}^\dagger F(x_k)\right|^2}{\sum_{k,j=1}^{3} U_{\mu k}U_{\mu k}^\dagger U_{el}U_{el}^\dagger},$$ (6.11)

where $F(x_k)$ is a loop function with $x_k = m_k^2 M_W^{-2}$. Since we assumed the heavy neutrinos to be mass-degenerate and the light neutrino mass is tiny compared to m_W we split the sum in the numerator into two parts with $F(0) = \frac{10}{3}$ and $F\left(\frac{M_N^2}{M_W^2}\right)$. Additionally we neglect the small deviation from one in the diagonal elements of $U_{\text{PMNS}} U_{PMNS}^\dagger$ in the denominator. Since the mixing matrix U is unitary we find

$$\frac{\Gamma(\mu \to e\gamma)}{\Gamma(\mu \to \nu_\mu e\bar\nu_e)} = \frac{3\alpha}{32\pi} \frac{\Delta m_\nu^2}{M_N^2} \left(F(0) - F\left(\frac{M_N^2}{M_W^2}\right) \right)^2$$
$$\times \left| \left(U_{\text{PMNS}} \frac{m_\nu}{\Delta m_\nu} U_{\text{PMNS}}^\dagger \right)_{\mu e} \right|^2. \quad (6.12)$$

Taking the best fit values from [29] we find $\left(U_{\text{PMNS}} \frac{m_\nu}{\Delta m_\nu} U_{\text{PMNS}}^\dagger \right)_{\mu e} = 0.12$. Thus, we can give the branching ratio as a function of the heavy neutrino mass only since the free parameters of the orthogonal matrix R cancel within this setup [15]. This expression is maximized for $M_N = 1.36 M_W$ and results in

$$\frac{\Gamma(\mu \to e\gamma)}{\Gamma(\mu \to \nu_\mu e\bar\nu_e)} = \frac{3\alpha}{32\pi} \frac{\Delta m_\nu^2}{M_W^2} 0.12^2 \cdot 0.266 \approx 10^{-31},$$
$$(6.13)$$

which is far below the experimental limit. For this reason, we also expect other LFV and electroweak precision observables not to significantly constrain the scenario.

Another imprint of this model could be found in additional decay channels of the Higgs if $M_N < m_h$. In this case the decays $h \to \nu_i N_j$ and $h \to N_i N_j$ are kinematically accessible. As pointed out in [10,38] the dominant contribution comes from the decay into a heavy and a light neutrino. However, branching ratios of this process larger than 10^{-2} are already ruled out and are typically much smaller due to the tiny Yukawa coupling [38]. Therefore, the contribution is negligible.

7 Conclusion

We have investigated a minimal neutrino portal DM model. The SM is extended by three right-handed neutrinos which generate the neutrino masses via a type I seesaw mechanism and, furthermore, act as mediator between the SM and DM. The dark sector consists of a boson ϕ and fermion χ coupled to the right handed neutrino via a Yukawa coupling. Motivated by the small Yukawa couplings of the type I seesaw mechanism in case of small heavy neutrino masses of $M_N \lesssim \mathcal{O}$ (PeV) we studied DM production via the freeze-in mechanism.

We derived analytic solutions for the number density in the resonant ($M_N > m_\chi + m_\phi$) and non-resonant ($M_N < m_\chi + m_\phi$) DM production regime. Adding the requirement that the coupling of the right-handed neutrino to the SM is of the same order of magnitude as its coupling to the dark sector allows for the prediction of the mediator or the DM mass respectively. In the non-resonant regime, we find $M_N \approx 10$ TeV. The non-resonant regime is studied in more detail numerically, as seen in Fig. 4.

Within the resonant regime, however, for $y_\chi \gtrsim y_\nu$ the resonant production of DM is strong enough to bring it into equilibrium with the SM. Thus, the freeze-out mechanism is recovered although the couplings between DM and the SM are feeble. Moreover, in this scenario we can predict a DM mass of $m_\chi \approx 100$ eV. For $y_\chi \ll y_\nu$, nonetheless, DM production via freeze-in is still possible. To satisfy the observed DM energy density the coupling of the right-handed neutrino to DM is required to be $y_\chi \approx 10^{-12} \sqrt{\frac{M_N}{m_\chi}}$.

The resonant scenario is strongly constrained by the measurement of the Lyman-α forest. The freeze-out case can be excluded completely, while freeze-in with $y_\chi \approx 10^{-12} \sqrt{\frac{M_N}{m_\chi}}$ is only viable for $m_\chi \gtrsim 3$ keV. Charged lepton flavor violation, Higgs decays, indirect detection and direct detection have little impact on our parameter space due to the feeble coupling of the SM to the dark sector. Thus, producing the observed DM energy density within this model of neutrino portal DM is possible even with small couplings between the SM and the dark sector.

Although within this work CP violation in the PMNS matrix was assumed to be absent, it could be included in the analysis to explore its phenomenological imprints and its impact on leptogenesis.

Appendix A: Boltzmann equations at the level of momentum distribution functions

A common simplifying assumption (e.g. in [17]) to solve the Boltzmann equation is to perform the momentum inte-

gration by assuming that if a particle distribution deviates from its equilibrium density it differs only by a momentum-independent factor, i.e. $f_i = \alpha_i f_i^{\text{th}}$ with $\frac{\partial \alpha_i}{\partial p_i} = 0$. Furthermore, the equilibrium densities of bosons and fermions are approximated by a Boltzmann distribution.

Following the lines of [26,39] we solve the Boltzmann equations at the level of momentum distribution functions. This has the advantage of a more accurate solution and the exact shape of the momentum distribution allows for more insights into the process of structure formation. Throughout the calculation we approximate the equilibrium densities of any particle species by a Boltzmann distribution. The Boltzmann equation is given by:

$$\left(\frac{\partial}{\partial t} - Hp \frac{\partial}{\partial p} \right) f(p, T(t)) = \mathcal{C}(p, T). \tag{A.1}$$

Here t is the time, H the Hubble parameter, f is the momentum distribution function of the particle species whose evolution is described by this Boltzmann equation, p is their momentum and $\mathcal{C}(p, T)$ is the collision term which describes the impact of interactions. For the integration of this equation it is convenient to perform a coordinate transformation $(t, p) \to (r, x)$ such that the differential operator on the left hand side contains a derivative with respect to one of the new variables only. If r only depends on t and

$$\frac{\partial x}{\partial t} - Hp(r, x) \frac{\partial x}{\partial p} = 0, \tag{A.2}$$

the L.H.S. of Eq. (A.1) results in

$$\frac{\partial r}{\partial t} \frac{\partial}{\partial r}. \tag{A.3}$$

The condition (A.2) is fulfilled if

$$x(p, t) = x \left(\frac{a(t)}{a(t_0)} p, t_0 \right) \tag{A.4}$$

A convenient choice for x is

$$x(p, t) = \frac{1}{T_0} \frac{a(t)}{a(t_0)} p = \left(\frac{g_s(T_0)}{g_s(T)} \right)^{\frac{1}{3}} \frac{p}{T}. \tag{A.5}$$

For the last equality we used the conservation of entropy $s(T_0)a(T_0) = s(T)a(T) = \text{const.}$ and g_s are the entropy degrees of freedom. The conservation of entropy also allows us to relate the temperature T to the time t:

$$\frac{dT}{dt} = -HT \left(1 + \frac{T}{3} \frac{dg_s}{dT} g_s^{-1} \right)^{-1}. \tag{A.6}$$

Since T is only a function of t and not of p we can choose

$$r(T) = \frac{m_0}{T}, \tag{A.7}$$

with m_0 being am arbitrary mass scale. Combining all this the Boltzmann equation results in

$$rH \left(1 - \frac{T}{3} \frac{\partial}{\partial r} \ln(g_s) \right)^{-1} \frac{\partial}{\partial r} f(p(r, x), T(r))$$
$$= \mathcal{C}(p(r, x), T(r)). \tag{A.8}$$

Since in this work DM production is mainly governed by $2 \leftrightarrow 2$ scattering processes we will discuss the collision term for these type of processes in more detail. For a $A + B \to C + DM$ scattering the collision term for the evolution of the momentum distribution function of DM is given by:

$$\mathcal{C}_{\mathcal{DM}}(p) = \frac{g_A g_B g_C}{2E_{DM}} \int \frac{d^3 \mathbf{p}_A}{2E_A (2\pi)^3} \frac{d^3 \mathbf{p}_B}{2E_B (2\pi)^3} \frac{d^3 \mathbf{p}_C}{2E_C (2\pi)^3}$$
$$\times (2\pi)^4 \delta^4 (p_A + p_B - p_C - p_{DM})$$
$$\times |\mathcal{M}|^2 (f_A f_B - f_C f_{DM}). \tag{A.9}$$

Here, $E_i = \sqrt{\mathbf{p}_i^2 + m_i^2}$, $\mathcal{M}$ is the matrix element for the process $A + B \to C + DM$ which is the same in both directions since we are assuming CP invariant interactions and f_i is the distribution function of particle species i. We assume that $f_C f_{DM} \ll f_A f_B$ which is justified since the paper explores the freeze in production of DM. Furthermore, we take $f_{A/B} = f_{A/B}^{th}$ assuming the interactions of A and B are efficient enough to keep them in thermal equilibrium. Moreover, taking $f_{A/B}^{th}$ to be a Boltzmann distribution, shifting the integration over $\mathbf{p}_c$ to $\mathbf{p}_C + \mathbf{p}_{DM} = \mathbf{P}$ and multiplying the equation by $1 = \int dP_0 \delta(P_0 - E_C - E_{DM})$ yields

$$\mathcal{C}(p_{DM}) = \frac{g_A g_B g_C}{4E_{DM}} \int \frac{d^4 P}{(2\pi)^3} \frac{exp(-P_0/T)}{E_C} \delta$$
$$\times (P_0 - E_C - E_{DM})$$
$$\times \int \frac{d^3 \mathbf{p}_A}{2E_A (2\pi)^3} \frac{d^3 \mathbf{p}_B}{2E_B (2\pi)^3} (2\pi)^4 \delta^4$$
$$\times (p_A + p_B - p_C - p_{DM})|\mathcal{M}|^2 \tag{A.10}$$

The equation above can be simplified by rewriting it in terms of the reduced cross section [40]:

$$g_A g_B g_C g_{DM} \int \frac{d^3 \mathbf{p}_A}{2E_A (2\pi)^3} \frac{d^3 \mathbf{p}_B}{2E_B (2\pi)^3} (2\pi)^4 \delta^4$$
$$\times (p_A + p_B - p_C - p_{DM})|\mathcal{M}|^2$$
$$= \frac{\hat{\sigma}(s)}{\sqrt{\left[1 - \frac{(m_C + m_{DM})^2}{s} \right] \left[1 - \frac{(m_C - m_{DM})^2}{s} \right]}}. \tag{A.11}$$

Moreover, we change the variables of integration from $d^4 P$ to an integration over the zero component of the center of mass momentum vector P_0, the center of mass energy s and the angle θ between center of mass momentum $\mathbf{P}$ and the momentum of the DM candidate $\mathbf{p}_{DM}$, $d^4 P = 2\pi \mathbf{P}^2 dP_0 d\mathbf{P} d\cos(\theta) = 2\pi \sqrt{P_0^2 - s} dP_0 ds d\cos(\theta)$. To

eliminate the remaining δ function we express the argument in terms of $\cos(\theta)$:

$$\delta\left(E_C + E_{DM} - P_0\right)$$
$$= \delta\left(\sqrt{\mathbf{P}^2 + \mathbf{p}_{DM}^2 - 2\mathbf{P}\mathbf{p}_{DM}\cos(\theta) + m_C^2} + E_{DM} - P_0\right)$$
$$= \frac{E_C}{\mathbf{P}\mathbf{p}_{DM}}\delta(\cos(\theta) - \cos(\theta_0)), \qquad (A.12)$$

where $\cos(\theta_0)$ is the value required for $\cos(\theta)$ for a vanishing argument of the δ function. Therewith, Eq. (A.10) results in

$$\mathcal{C}(p_{DM}) = \frac{1}{4g_{DM}E_{DM}\mathbf{p}_{DM}}\int_{s_{\min}}^{\infty} ds$$
$$\times \frac{\hat{\sigma}(s)}{\sqrt{\left[1 - \frac{(m_C + m_{DM})^2}{s}\right]\left[1 - \frac{(m_C - m_{DM})^2}{s}\right]}}$$
$$\times \int_{\sqrt{s_{\min}}}^{\infty} \frac{dP_0}{(2\pi)^2}\exp\left(-\frac{P_0}{T}\right)$$
$$\times \underbrace{\int_{-1}^{1} d\cos(\theta)\,\delta\left(\cos(\theta) - \cos(\theta_0)\right)}_{=1,\ \text{if}\ \cos(\theta_0)\in[-1,1]} \qquad (A.13)$$

The last integral basically restricts the boundaries of either P_0 or s in the sense that if

$$\sqrt{\mathbf{P}^2 + \mathbf{p}_{DM}^2 - 2\mathbf{P}\mathbf{p}_{DM}\cos(\theta_0) + m_C^2} + E_{DM} - P_0 = 0 \qquad (A.14)$$

is fulfilled $|\cos(\theta_0)| \le 1$ must hold. This requirement yields the inequality

$$(s + m_{DM}^2 - m_C^2 - 2P_0 E_{DM})^2 \le 4\mathbf{p}_{DM}^2(P_0^2 - s). \qquad (A.15)$$

In case of $m_C = m_{DM}$[9] this results in a lower (relative minus sign) and upper bound (relative plus sign) of the P_0 integration of

$$P_0^{\pm} = \frac{E_{DM}s}{2m_{DM}^2}\left[1 \pm \frac{p_{DM}}{E_{DM}}\sqrt{1 - 4\frac{m_{DM}^2}{s}}\right]$$
$$\overset{m_{DM}=0}{=}\begin{cases} P_0^+ \to \infty \\ P_0^- = \frac{s}{4p_{DM}} + p_{DM} \end{cases}. \qquad (A.16)$$

---

[9] This is a good approximation for this work since we assume the dark sector to be almost degenerate in mass.

The last equality is given to showcase that in case of $m_{DM} = 0$ only a lower bound exists, as was shown in [39], while for finite DM masses there is also an upper bound. Thus, we have

$$\mathcal{C}(p_{DM}) = \frac{1}{4g_{DM}E_{DM}\mathbf{p}_{DM}}\int_{s_{\min}}^{\infty} ds$$
$$\times \frac{\hat{\sigma}(s)}{\sqrt{1 - 4\frac{m_{DM}^2}{s}}}\int_{P_0^-}^{P_0^+} \frac{dP_0}{(2\pi)^2}\exp\left(-\frac{P_0}{T}\right). \qquad (A.17)$$

The s integral and the following integration of the differential equation for an arbitrary cross section cannot be performed analytically. However, in case of a very light DM candidate ($m_{DM} \approx 0$) and a resonant production process with $\Gamma_{\text{mediator}} \ll M_{\text{mediator}}$ the integral can be evaluated analytically. Moreover, this case is of special interest for this work since for resonant production the DM mass turns out to be below keV. Therefore, the exact shape of the momentum distribution is required to quantify the impact of DM on structure formation. In this case we have $P_0^+ \to \infty$ and

$$\hat{\sigma}(s) \approx \delta(s - M_N^2)\sqrt{1 - 4\frac{m_{DM}^2}{s}}\hat{\sigma}_{BW}(s). \qquad (A.18)$$

Hence the collision term yields

$$\mathcal{C}(p_{DM}) = \frac{T}{32\pi^2 g_{DM}\mathbf{p}_{DM}^2}\hat{\sigma}_{BW}(M_N^2)$$
$$\exp\times\left(-\frac{M_N^2}{4\mathbf{p}_{DM}T} - \frac{\mathbf{p}_{DM}}{T}\right). \qquad (A.19)$$

Transforming the variables according to Eqs. (A.7) and (A.5) and taking g_s to be a constant, i.e. $x = \frac{\mathbf{p}_{DM}}{T}$, leads to

$$\mathcal{C}(p_{DM}) = \frac{1}{32\pi^2 g_{DM}}\frac{r}{x^2 m_0}\hat{\sigma}_{BW}(M_N^2)$$
$$\exp\times\left(-\frac{M_N^2 r^2}{4x m_0^2} - x\right). \qquad (A.20)$$

A collision term of this form can be integrated and results in the following momentum distribution function:

$$f(p, T) = \frac{M_{pl}\hat{\sigma}_{BW}(M_N^2)}{64\pi^2 g_{DM}c_H}\frac{\exp(-p/T)}{M_N^3}\frac{T^2}{p^2}$$
$$\times\left[\sqrt{\frac{\pi p}{T}}\,\text{erf}\left(\frac{M_N}{\sqrt{pT}}\right) - 2\frac{M_N}{T}\exp\left(-\frac{M_N^2}{Tp}\right)\right], \qquad (A.21)$$

where $\text{erf}(x)$ is the error function. Therewith, the number density is given by the integration over the momentum

$$n(T) = 4\pi g_{DM} \int_0^\infty p^2 f(p,T) \stackrel{T \ll M_N}{=} \frac{M_{pl} \hat{\sigma}_{BW}(M_N^2)}{8 c_H} \frac{T^3}{M_N^3}.$$

(A.22)

In the last step, we assumed that the temperature where we observe the DM density is much smaller than the mass of the resonant particle. As mentioned above, to derive this analytic result we took the effective entropy degrees of freedom to be a constant. Hence the above formula is only a good approximation as long as we take T large enough to stay at a constant value of $g_s(T) \approx 100$. Of course, we observe the universe at a smaller temperature. However, the above result remains a good approximation if the main part of the production has been finished before $g_s(T)$ starts to vary significantly since for a collisionless particle species the quantity $Y = \frac{n}{s}$ is a constant.

By comparing the number of produced DM particles at temperature T to the number of particles for $T \to 0$, $\frac{n(T)T^3}{\lim_{T \to 0} n(T)T^3}$, with an unapproximated $n(T)$ we find that for $T \approx \frac{M_N}{4}$ already over 0.99 of DM particle have been produced. Thus, as long as $M_N \geq 100$ GeV the result (A.22) serves as a good estimate.

Beside collision terms for $2 \leftrightarrow 2$ scattering processes, the collision term for the (inverse) decay $N \leftrightarrow vh$ is required. The procedure for performing the integration over the particle momenta follows the same lines as for the $2 \leftrightarrow 2$ scattering. Thus, we only give the result for the collision term resulting from the decay that appears in the Boltzmann equation for the heavy neutrino N:

$$C_N(p_N) = \frac{M_N}{\sqrt{p_N^2 + M_N^2}} \left[\frac{y_v^2 g_v g_h}{16\pi} M_N \exp\left(-\frac{\sqrt{p_N^2 + M_N^2}}{T} \right) \right.$$

$$\left. - \Gamma_{N \to vh} f_N(p_N, T) \right].$$

(A.23)

Appendix B: Cross sections

Here, we give the relevant reduced cross sections for the case $m_\phi = m_\chi$. Since CP conservation is assumed the reduced cross sections for a process and its time reserved process are the same.

$$\hat{\sigma}_{v_i h \leftrightarrow \chi\phi}(s) = \left(\sum_j (Y_v)_{ij} y_\chi \right)^2 \frac{\left(1 - \frac{m_h^2}{s} \right)^2}{32\pi}$$

$$\times \frac{s^2 \sqrt{1 - 4\frac{m_\chi^2}{s}}}{(s - M_N^2)^2 + \Gamma_N^2 M_N^2}$$

(B.1)

Here, Γ_N is the total decay width of the propagating neutrino which can decay into vh for $M_N > m_h$ and into $\chi\phi$ for $M_N > 2m_\chi$. The decay width is given by:

$$\Gamma_N = y_v^2 \frac{(M_N^2 - m_h^2)^2}{16\pi M_N^3} + y_\chi^2 \frac{(M_N + 2m_\chi)\sqrt{M_N^2 - 4m_\chi^2}}{16\pi M_N}.$$

(B.2)

$$\sigma_{Wl \to \chi\phi} = y_\chi^2 y_v^2 \frac{3M_W^2}{24\pi s M_N (s - M_W^2)^2} [(M_W^2 - m_l^2)(M_W^2$$

$$+ 2(m_l^2 - M_W^2) - 4M_N m_\chi)$$

$$+ (M_N^2 + m_l^2 - M_W^2 + 4M_N m_\chi)]$$

$$\times \sqrt{\frac{s(s - 4m_\chi^2)}{m_l^4 + (s - M_W^2)^2 - 2m_l^2(s + M_W^2)}}$$

(B.3)

$$\sigma_{Zv \to \chi\phi} = y_\chi^2 y_v^2 \frac{3M_W^2 \sqrt{1 - \frac{4m_\chi^2}{s}}}{16\pi^2 M_Z^2 (s - M_N^2)(s - M_Z^2)}$$

$$\times [(s + M_Z^2)M_N^2 + 4M_N m_\chi (s - M_Z^2)$$

$$+ s^2 - s M_Z^2 - 2M_Z^4]$$

(B.4)

$$\hat{\sigma}_{NN \to \chi\chi} = \frac{y_\chi^4}{32\pi s} \left[\frac{\sqrt{(s - 4m_\chi^2)(s - 4M_N^2)}(2M_N^4 - 4M_N^2 m_\chi^2 + m_\chi^2 s)}{M_N^4 - 4M_N^2 m_\chi^2 + m_\chi^2 s} \right.$$

$$\left. - 4M_N^2 \operatorname{arcCoth}\left(\frac{2M_N^2 - s}{\sqrt{(s - 4m_\chi^2)(s - 4M_N^2)}} \right) \right]$$

(B.5)

$$\sigma_{NN \to \phi\phi} = y_\chi^4 \left(1 - \frac{4m_\chi^2}{s} \right) \left[-\sqrt{(s - 4M_N^2)(s - 4m_\chi^2)} \right.$$

$$\times (m_\chi^2 s + 2M_N^4 + 4M_N^3 m_\chi)$$

$$+ 2[2M_N(2m_\chi M_N) + s][m_\chi^2(s - 4M_N^2) + M_N^4]$$

$$\left. \times \operatorname{arctanh}\left(\frac{\sqrt{(s - 4M_N^2)(s - 4m_\chi^2)}}{s - 2M_N^2} \right) \right]$$

(B.6)

References

1. S.-L. Chen, Z. Kang, JCAP **1805**, 036 (2018). arXiv:1711.02556
2. L.J. Hall, K. Jedamzik, J. March-Russell, S.M. West, JHEP **03**, 080 (2010). arXiv:0911.1120
3. N. Bernal, M. Heikinheimo, T. Tenkanen, K. Tuominen, V. Vasko-nen, Int. J. Mod. Phys. A **32**, 1730023 (2017). arXiv:1706.07442
4. S. Dodelson, L.M. Widrow, Phys. Rev. Lett. **72**, 17 (1994). arXiv:hep-ph/9303287
5. K. Perez et al., Phys. Rev. D **95**, 123002 (2017). arXiv:1609.00667
6. M.D. Campos, F.S. Queiroz, C.E. Yaguna, C. Weniger, JCAP **1707**, 016 (2017). arXiv:1702.06145
7. T. Asaka, M. Laine, M. Shaposhnikov, JHEP **01**, 091 (2007). arXiv:hep-ph/0612182 [Erratum: JHEP **02**, 028 (2015)]
8. M. Drewes et al., JCAP **1701**, 025 (2017). arXiv:1602.04816
9. M. Escudero, N. Rius, V. Sanz, JHEP **02**, 045 (2017). arXiv:1606.01258

10. M. Escudero, N. Rius, V. Sanz, Eur. Phys. J. C **77**, 397 (2017). arXiv:1607.02373
11. M.G. Folgado, G.A. Gómez-Vargas, N. Rius, R. Ruiz De Austri JCAP **1808**, 002 (2018). arXiv:1803.08934
12. B. Batell, T. Han, D. McKeen, B. Shams Es Haghi, Phys. Rev. D **97**, 075016 (2018). arXiv:1709.07001
13. A. Merle, M. Platscher, Phys. Rev. D **92**, 095002 (2015). arXiv:1502.03098
14. M. Lindner, M. Platscher, C.E. Yaguna, A. Merle, Phys. Rev. D **94**, 115027 (2016). arXiv:1608.00577
15. J.A. Casas, A. Ibarra, Nucl. Phys. B **618**, 171 (2001). arXiv:hep-ph/0103065
16. A. Pilaftsis, Z. Phys. C **55**, 275 (1992). arXiv:hep-ph/9901206
17. G.F. Giudice, A. Notari, M. Raidal, A. Riotto, A. Strumia, Nucl. Phys. B **685**, 89 (2004). arXiv:hep-ph/0310123
18. Particle Data Group, C. Patrignani et al., Chin. Phys. C **40**, 100001 (2016)
19. M. Blennow, E. Fernandez-Martinez, B. Zaldivar, JCAP **1401**, 003 (2014). arXiv:1309.7348
20. N. Arkani-Hamed, S. Dimopoulos, G.R. Dvali, J. March-Russell, Phys. Rev. D **65**, 024032 (2001). arXiv:hep-ph/9811448
21. M. Becker, H. Pas, Eur. Phys. J. C **78**, 273 (2018). arXiv:1707.02882
22. S. Tremaine, J.E. Gunn, Phys. Rev. Lett. **42**, 407 (1979). [66 (1979)]
23. J. Baur et al., JCAP **1712**, 013 (2017). arXiv:1706.03118
24. Particle Data Group, M. Tanabashi et al., Phys. Rev. D **98**, 030001 (2018)
25. M. Garny, J. Heisig, Phys. Rev. D **98**, 095031 (2018). arXiv:1809.10135
26. J. Konig, A. Merle, M. Totzauer, JCAP **1611**, 038 (2016). arXiv:1609.01289
27. Planck, N. Aghanim et al., (2018). arXiv:1807.06209
28. T.A. Chowdhury, S. Nasri, Phys. Rev. D **97**, 075042 (2018). arXiv:1801.07199
29. I. Esteban, M.C. Gonzalez-Garcia, A. Hernandez-Cabezudo, M. Maltoni, T. Schwetz, JHEP **01**, 106 (2019). arXiv:1811.05487
30. M. Escudero, A. Berlin, D. Hooper, M.-X. Lin, JCAP **1612**, 029 (2016). arXiv:1609.09079
31. A. Berlin, D. Hooper, S.D. McDermott, Phys. Rev. D **89**, 115022 (2014). arXiv:1404.0022
32. T. Hambye, M.H.G. Tytgat, J. Vandecasteele, L. Vanderheyden, Phys. Rev. D **98**, 075017 (2018). arXiv:1807.05022
33. XENON, E. Aprile et al., Phys. Rev. Lett. **119**, 181301 (2017). arXiv:1705.06655
34. B. Batell, T. Han, B. Shams Es Haghi, Phys. Rev. D **97**, 095020 (2018). arXiv:1704.08708
35. S. Antusch, O. Fischer, JHEP **10**, 094 (2014). arXiv:1407.6607
36. E. Molinaro, J. Phys. Conf. Ser. **447**, 012052 (2013). arXiv:1303.5856
37. S. Antusch, C. Biggio, E. Fernandez-Martinez, M.B. Gavela, J. Lopez-Pavon, JHEP **10**, 084 (2006). arXiv:hep-ph/0607020
38. A.M. Gago, P. Hernandez, J. Jones-Perez, M. Losada, A. Moreno Briceno, Eur. Phys. J. C **75**, 470 (2015). arXiv:1505.05880
39. J. Heeck, D. Teresi, Phys. Rev. D **96**, 035018 (2017). arXiv:1706.09909
40. M.A. Luty, Phys. Rev. D **45**, 455 (1992)